Electrochimica Acta 178 (2015) 80–91

Contents lists available at ScienceDirect

Electrochimica Acta

journal homepage: www.elsevier.com/locate/electacta

Nickel-*N,N'–bis*(salicylidene)-1,3-propanediamine (Ni-*Salpn*) film-modified electrodes. Influence of electrodeposition conditions and of electrode material on electrochemical behaviour in aqueous solution

Cibely S. Martin[a,b], Carla Gouveia-Caridade[b], Frank N. Crespilho[c], Carlos J.L. Constantino[a], Christopher M.A. Brett[b,*]

[a] *Departamento de Física, Química e Biologia, Faculdade de Ciências e Tecnologia, UNESP Univ Estadual Paulista, Presidente Prudente-SP, Brazil*
[b] *Department of Chemistry, Faculty of Sciences and Technology, University of Coimbra, 3004-535 Coimbra, Portugal*
[c] *Instituto de Química de São Carlos, Universidade de São Paulo, São Carlos-SP, Brazil*

ARTICLE INFO

Article history:
Received 11 June 2015
Received in revised form 20 July 2015
Accepted 21 July 2015
Available online 26 July 2015

Keywords:
Ni-*Salpn* films
Electrodeposition
Influence of electrode material
EQCM
UV-vis and Raman spectroscopy

ABSTRACT

Modified electrodes based on films of *Schiff* base complexes are excellent candidates for sensing applications. The influence of the electrode material, glassy carbon, platinum, gold or indium tin oxide, on the electrodeposition of nickel-*N,N'–bis*(salicylidene)-1,3-propanediamine (Ni-*Salpn*) films in 1,2-dichloroethane (DCE) was investigated, and their electrochemical behaviour was evaluated by cyclic voltammetry and electrochemical impedance spectroscopy. The effect of the electrodeposition potential and electrodeposition time on the electrochemical behaviour of Ni-*Salpn* was examined using glassy carbon as substrate. The film growth process was investigated using the electrochemical quartz crystal microbalance and UV-vis absorption spectroscopy and structural differences between the Ni-*Salpn* complex and the Ni-*Salpn* film were examined by micro-Raman spectroscopy. The results demonstrate that the electrodeposition mechanism is independent of the electrode material, but that the nature of the substrate material influences the rate of film growth, the electrochemical behaviour and the stability of the film-modified electrodes in aqueous solution. Counteranion insertion during oxidation can break the bonds between the complexes in the stacked Ni-*Salpn* film structure and cause both mass loss and blockage of the redox metal centre activity, but these effects are small in thin films.

1. Introduction

Metal-*Schiff* complexes with tetradentate N_2O_2 ligands are being widely studied as modifiers of electrodes by oxidative electrodeposition on a variety of conducting surfaces [1–4]. The electrodeposition mechanism has been extensively discussed in the literature by Goldsby *et al.* [5,6] and Audebert *et al.* [7–9], in which radical-radical coupling was proposed. However, Vilas-Boas *et al.* [10,11] and Dahm *et al.* [12] concluded that the mechanism is based on the interactions between the phenol ring and the metallic centre with formation of Ni-phenyl stacks. Nevertheless, in both hypotheses, the films are classified as conducting due to the donor sites (metallic centre) and delocalized redox moieties (π-conjugated system), where electron transfer occurs at the metallic centres, leading to important applications in electrochemical sensors [4,13–15]. The properties of *Schiff* films depend on the electrodeposition conditions, such as structure of the monomer [16,17], electrodeposition mode [18,19], potential range, fixed applied potential or current [19], the nature of the electrode material [12], and solvent [5]. Thus, characterization *in situ* is very important for understanding the electrochemical behaviour of the film formed and its interactions with the electrode surface as well as with species present in solution.

Among the metal-*Schiff* complexes, the nickel *N,N'–bis*(salicylidene)-1,3-propanediamine complex (Ni-*Salpn*) has been used as an antimicrobial agent [20] and as a chelating agent in complexometric potentiometric titrations [21]. Ni-*Salpn* was first electrodeposited by Ardasheva *et al.* [19] on platinum electrodes. Since then, no reports on electrodeposited Ni-*Salpn* are found in the literature; only a few studies concerning the ligand *Salpn* in other soluble metal complexes have been reported [22,23]. To our knowledge, the influence of the electrode substrate material

* Corresponding author. Tel.: +351 239854470; fax: +351 239827703.
E-mail address: cbrett@ci.uc.pt (C.M.A. Brett).

http://dx.doi.org/10.1016/j.electacta.2015.07.123
0013-4686/

and electrodeposition parameters with a view to optimisation for sensor applications has not been evaluated.

In this work, the electrodeposition of Ni-*Salpn* was carried out in 1,2-dichlorethane (DCE) on four different types of electrode substrate, i.e. glassy carbon, platinum, gold and indium tin oxide (ITO), in order to evaluate the influence of electrode material on the electrodeposition process as well as on the electrochemical and electrical properties of the film-modified electrodes in aqueous solution.

The electrodeposition process and the electrochemical behaviour of the Ni-*Salpn* films in aqueous solution were evaluated by cyclic voltammetry, a useful tool to investigate catalytic mechanisms and structure-reactivity relationships [24–26]. In addition, electrochemical impedance spectroscopy (EIS) was used to investigate the electrical properties and electron transfer [27–29] resulting from Ni-*Salpn*/substrate and/or Ni-*Salpn*/solution interface interactions. Characterization of film growth was carried out by the electrochemical quartz crystal microbalance (EQCM) and UV-vis absorption spectroscopy. Micro-Raman spectroscopy was used to evaluate the structural or chemical changes between the Ni-*Salpn* complex and Ni-*Salpn* films.

2. Experimental

2.1. Reagents and solutions

The Ni-*Salpn* complex (nickel-*N,N'–bis*(salicylidene)-1,3-propanediamine) was prepared from *N,N'–bis*(salicylidene)-1,3-propanediamine ligand (Sigma-Aldrich) and nickel acetate (Sigma-Aldrich), as previously described in the literature [30]. The electrodeposition process was carried out using a 1.0 mmol L^{-1} Ni-*Salpn* solution prepared in 1,2 -dichloroethane (DCE, Sigma-Aldrich) containing 0.1 mol L^{-1} tetrabutylammonium perchlorate (TBAP, Fluka) as supporting electrolyte.

Electrochemical measurements of the modified electrodes were done in 0.1 mol L^{-1} potassium chloride (KCl, Fluka) aqueous solution, prepared with Millipore Milli-Q nanopure water (resistivity ≥ 18 MΩ cm).

2.2. Instrumentation and methods

Glassy carbon, (GC - 0.28 cm^2), platinum (Pt–0.0628 cm^2), gold (Au–0.00785 cm^2) and indium tin oxide (ITO ~ 1.0 cm^2), were used as working electrodes. All electrochemical experiments were performed in a conventional three-electrode cell, using an Ag/AgCl (sat. KCl) electrode as reference and a platinum wire as counter electrode.

Cyclic voltammetry experiments were carried out using an Ivium CompactStat.e potentiostat (Ivium Technologies, Utrecht, Netherlands). Electrochemical impedance spectroscopy (EIS) experiments were carried out at open circuit potential (OCP) using a Solartron 1250 Frequency Response Analyser, coupled to a Solartron 1286 Electrochemical Interface (Solartron Analytical, UK) controlled by Zplot Software. Impedance spectra were analysed by fitting to equivalent circuits using ZView Software (Scribner Associates, USA). A sinusoidal voltage perturbation of amplitude 10 mV rms was applied in the frequency range from 65000 Hz to 0.1 Hz with 10 frequency steps per decade, and integration time 60s.

The Ni-*Salpn* electrodeposition process and evaluation of the physical stability of the films formed in aqueous solution were followed gravimetrically, using an electrochemical quartz crystal microbalance (EQCM), eQCM 10M™ Quartz Crystal Microbalance, Gamry Instruments, with AT-cut Au-coated piezoelectric quartz crystals (AuQC) with 10 MHz resonance frequency.

Characterization by UV-vis absorption and micro-Raman spectroscopy was performed using modified ITO electrodes. UV-vis absorption spectroscopy was carried out using a Varian model Cary 50 spectrophotometer (Varian, USA), and Raman spectra were obtained with a Renishaw model in-Via micro-Raman spectrograph (Renishaw, UK), coupled to a Leica optical microscope.

2.3. Electrodeposition of Ni-Salpn films

Ni-*Salpn* films were electrodeposited in both potentiodynamic and potentiostatic modes on the various electrode materials. Potentiodynamic electrodeposition was carried out in a solution in DCE containing 1 mmol L^{-1} Ni-*Salpn* complex in 0.1 mol L^{-1} TBAP by potential cycling between 0.0 and +1.4 V *vs.* Ag/AgCl at 50 mV s^{-1}. Potentiostatic electrodeposition was performed in a solution of the same composition at a constant potential of +1.2 *vs.* Ag/AgCl for 900 s. The influence of varying the electrodeposition conditions was assessed using a GC working electrode, where the Ni-*Salpn* films were obtained at different electrodeposition potentials (+1.0, +1.1 and +1.2 V *vs.* Ag/AgCl at 900 s), also varying the electrodeposition time (300, 600, 900 and 1200 s at +1.2 V *vs.* Ag/AgCl).

All electrochemical measurements of the film-modified electrodes were carried out under a nitrogen atmosphere.

Gravimetric measurements during the electrodeposition process performed at +1.2 V *vs.* Ag/AgCl for 300 and 900 s, were done using a gold-coated quartz crystal (AuQC–0.205 cm^2) as electrode substrate.

UV-vis and micro-Raman characterization was done with an ITO electrode modified with the Ni-*Salpn* film electrodeposited at a constant potential of +1.2 V *vs.* Ag/AgCl for a fixed time of 300 or 900 s.

2.4. Characterization of Ni-Salpn films in aqueous solution

After each modification stage, the electrode modified with Ni-*Salpn* film was washed thoroughly with Millipore Milli-Q nanopure water and allowed to dry at room temperature for one hour. All characterizations in aqueous solution were carried out using a 0.1 mol L^{-1} KCl solution. Cyclic voltammetry measurements were done at 25 mV s^{-1} in the potential range 0.1 to 0.8 V *vs.* Ag/AgCl. The potential cycling was also followed gravimetrically in the same experimental conditions. In addition, the modified electrodes were characterized by EIS at OCP using 0.1 mol L^{-1} KCl solution.

The influence of anion on electrochemical stability of thinner film in aqueous solution was studied using various supporting electrolytes of concentration 0.1 mol L^{-1} with the same cation (Na^+) and different anions: Cl^-, NO_3^-, ClO_4^-, SO_4^{2-}.

3. Results and Discussion

3.1. Formation and voltammetric behaviour of Ni-Salpn films on different electrode materials

Ni-*Salpn* films were obtained by potential cycling in a solution of 1 mmol L^{-1} Ni-*Salpn* in 0.1 mol L^{-1} TBAP/DCE between 0.0 and +1.4 V *vs.* Ag/AgCl at 50 mV s^{-1}, and then characterised by cyclic voltammetry in 0.1 mol L^{-1} KCl aqueous solution.

3.1.1. Deposition of Ni-salpn films

The increasing anodic and cathodic peak currents with increasing number of cycles due to growth of the Ni-*Salpn* film was observed for all electrode materials, as shown in Fig. 1. The increase of the anodic-cathodic peak potential separation (ΔE_p) indicates a decrease of electrochemical activity of the Ni-*Salpn* complex that makes formation of subsequent layers more difficult [31]. On gold electrode substrates, a decrease in the peak current after ten cycles

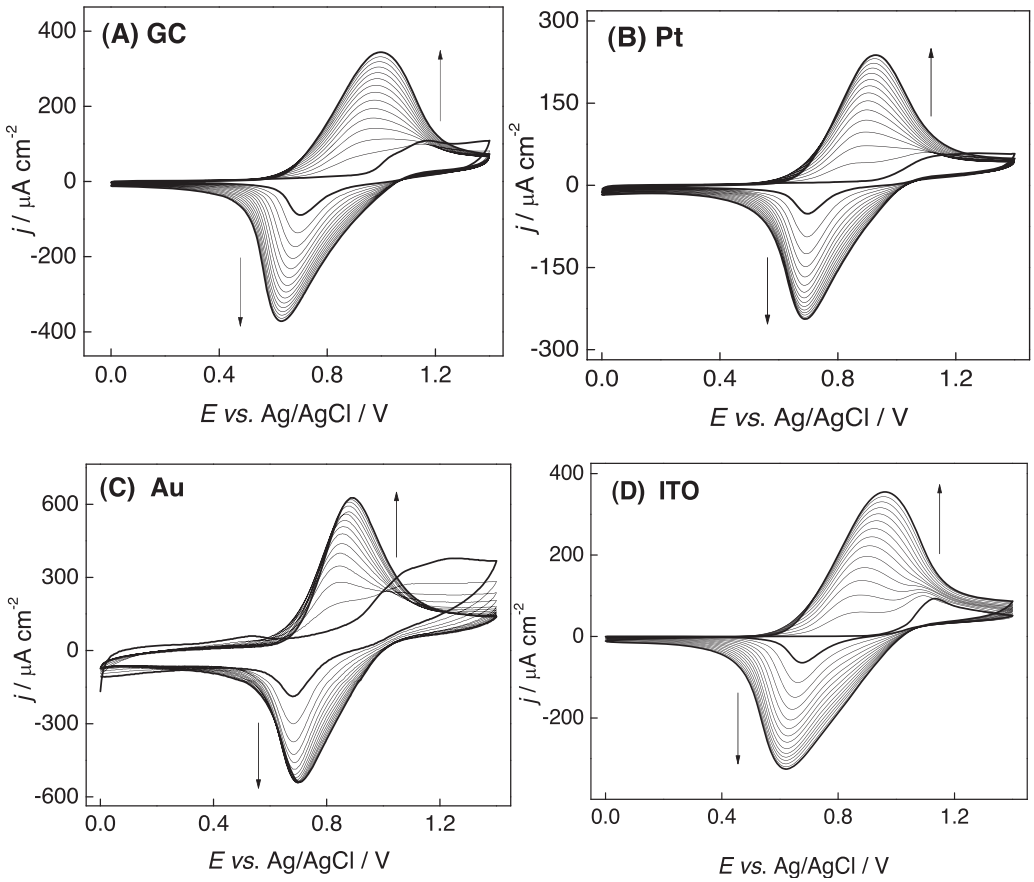

Fig. 1. Cyclic voltammetric response for the electrodeposition of 1.0 mmol L^{-1} Ni-*Salpn* in 0.1 mol L^{-1} TBAP/DCE on (A) GC, (B) Pt, (C) Au and (D) ITO electrodes, applying 15 potential cycles between 0.0 and +1.4 V *vs.* Ag/AgCl at 50 mV s^{-1}.

was observed, which can be ascribed to the decreasing redox activity of Ni-*Salpn* films due to irreversible oxidation of ligand [10,19], to solvent decomposition or to other reactions from adsorption of intermediates/dimers present in solution [32]. For GC, Pt and ITO electrodes, a decrease of peak current appears only after 30 potential cycles. Such differences in behaviour demonstrate that the electrode material can influence the amount of the Ni-*Salpn* film electrodeposited on the electrode surface (film growth).

The electrodeposition mechanism of Ni-*Salpn* begins with electron transfer from a ligand-centred orbital. An irreversible anodic wave corresponding to oxidation of the Ni-*Salpn* complex with formation of the cation radical, and a quasi-reversible process at less positive potentials, attributed to the Ni(II)/Ni(III) redox couple [5], was observed in the first potential scan. After Ni-*Salpn* oxidation, the oxidized species react rapidly with other monomers present in solution forming a stacked acceptor-donor deposit on the electrode surface [10,12]. Visual inspection of the electrodes showed the deposition of a green film, similar to other nickel-*Schiff* complexes in the literature [10,12,14].

Table 1 summarizes the parameters obtained from the cyclic voltammograms in Fig. 1. It can be seen that there are differences in the potential for cation radical formation and of the redox couple Ni(II)/Ni(III), as well as changes in the peak current for the electrodeposition process, all depending on the identity of the substrate electrode. This can be attributed to the intrinsic properties of the electrode material such as porosity and reactivity of the surface, which directly influence not only the potential of cation radical formation and overoxidation of Ni-*Salpn*, but also the organization of ions and solvent on the electrode surface [32]. The electrode material can determine the rate of monomer adsorption and the kinetics and growth mechanism of the film, and thence the stability of the film on the electrode surface.

Ni-*Salpn* films were also obtained by applying a constant fixed potential of +1.2 V *vs.* Ag/AgCl during 900 s (potentiostatic mode). However, formation at constant fixed potential leads to the deposition of thick films more rapidly than cycling the potential (potentiodynamic mode).

Thus, the electrode material has little influence on the mechanism of Ni-*Salpn* formation, but plays an important role in the amount of film electrodeposited (thickness).

3.1.2. *Cyclic voltammetry of Ni-*salpn *film modified electrodes in aqueous solution*

The voltammetric profile of the modified electrodes in 0.1 mol L^{-1} KCl solution, exhibits only one redox process attributable to the Ni(II)/Ni(III) redox couple, Fig. 2a, but the midpoint potential and quasireversibility (ΔE value) was different for

Table 1
Peak potentials in the Ni-*Salpn* potential cycling electrodeposition process on different electrode materials in the 15th potential cycle; solution of 1.0 mmol L^{-1} Ni-*Salpn* in 0.1 mol L^{-1} TBAP/DCE. E_{cr}, potential for cation radical formation; E_{pa}, anodic peak potential; E_{pc}, cathodic peak potential. Potential values vs. Ag/AgCl.

Substrate	E_{cr}/V	Ni(II)/Ni(III)		ΔE_p/V
		E_{pa}/V	E_{pc}/V	
GC	1.16	0.997	0.629	0.368
Pt	1.28	0.927	0.688	0.239
Au	1.23	0.890	0.704	0.186
ITO	1.13	0.963	0.619	0.344

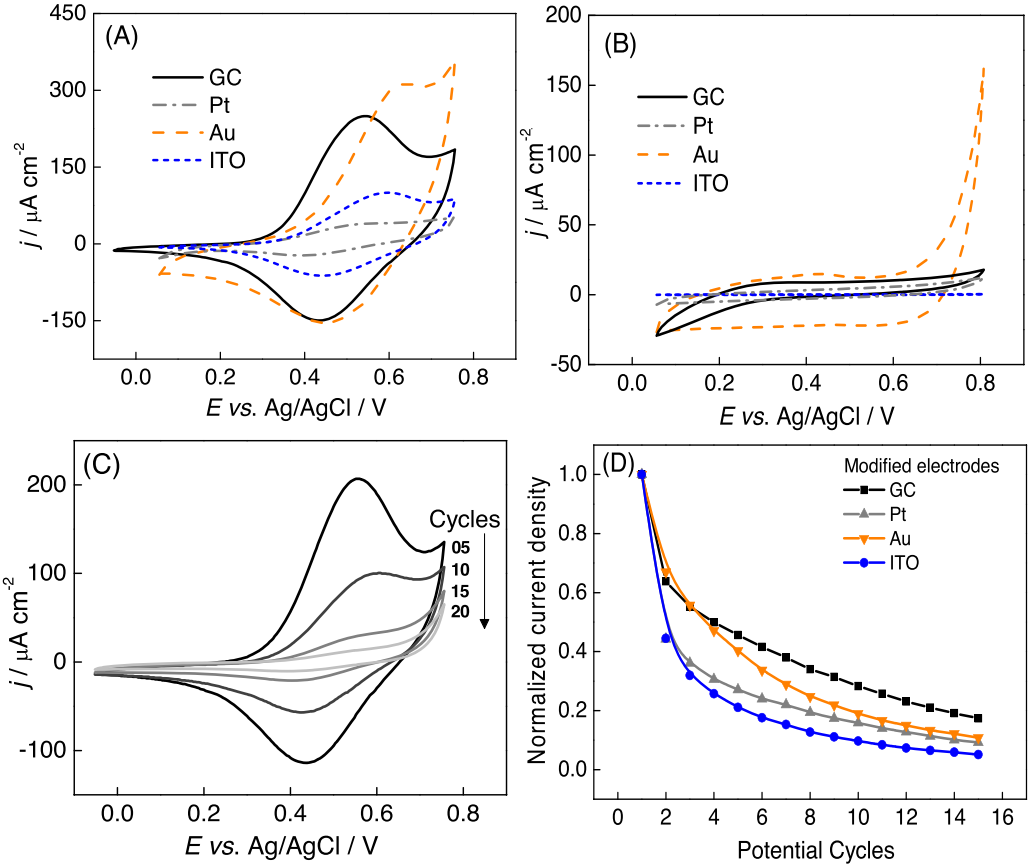

Fig. 2. Cyclic voltammetry in 0.1 mol L^{-1} KCl aqueous solution; $v = 25$ mV s^{-1}; third cycle, for GC, Pt, Au and ITO electrodes (A) modified with Ni-*Salpn* and (B) unmodified. (C) Voltammetric response during cycle 5, 10, 15 and 20 for GC electrode substrate (D) Variation of current density with number of potential cycles for modified GC, Pt, Au and ITO electrode substrates.

each electrode material. The peak potential values obtained from the third cycle are presented in Table 2. The GC electrode modified with Ni-*Salpn* film showed the smallest ΔE value, suggesting that electron transfer between the Ni-*Salpn* film and electrode surface is faster than for the Pt, Au and ITO electrode substrates, and is related with the amount of film electrodeposited.

Furthermore, for the same deposition parameters on different substrates, Ni-*Salpn* films with different thicknesses were obtained, which supports the hypothesis that the electrode material influences the rate of film growth. The theoretical thickness, *l*, of the Ni-*Salpn* film was estimated for each modified electrode using the equation derived from the Faraday's law:

$$l = \frac{MQ}{nFA\rho}$$

where *M* is the molecular mass of the monomer (339.02 g mol^{-1}), *Q* is the charge, calculated by the integration of the anodic peak obtained from the cyclic voltammogram in KCl ($v = 25$ mV s^{-1}), *n* is the number of electrons transferred (assumed to be 1), *F* the Faraday constant (96485 C mol^{-1}), *A* the electrode area (in cm^2) and ρ the film density (~1 g cm^{-3}) [4]. The Ni-*Salpn* film thicknesses were: 41 nm on the GC electrode, 18 nm, 12 nm and 2.8 nm for the Au, ITO and Pt electrodes, respectively.

The modified GC electrode showed the greatest film thickness, and highest electron transfer rate (smallest ΔE). These variations in behaviour occur due to the specific interaction between the Ni-*Salpn* film and the electrode material.

The Ni-*Salpn* films are unstable in aqueous solution, since the peak currents decrease with increasing number of cycles as shown in Fig. 2b. After 15 potential cycles, the peak currents were approximately equal to those of the bare electrode, where no redox activity was observed. However, visual inspection showed that the Ni-*Salpn* film remained on the electrode surface, which suggests that changes in the film structure cause blocking of the electrode surface.

A possibility is the formation of nickel oxides and/or hydroxides, that lead to loss of redox activity [32]. In addition, ion diffusion from bulk electrolyte to inside the Ni-*Salpn* film may block the redox process, through complexation of nickel centres with species from solution (chloride ion and/or water ligand). However, this behaviour has not been discussed in the literature, and so EIS and gravimetric measurements were performed to better understand the behaviour of the modified electrode (see below).

A smaller peak current due to oxidation of the Ni-*Salpn* film was observed on Pt and Au, since metallic materials can form oxides in aqueous solutions at potentials less positive than carbon and conductive oxides [32–34], decreasing the rate of charge

Table 2
Anodic and cathodic peak potentials from cyclic voltammograms obtained in 0.1 mol L^{-1} KCl solution for the Ni-*Salpn* film on different electrode substrates; values for 3rd cycle. Potential values vs. Ag/AgCl.

Substrate	Ni(II)/Ni(III)		Ni(II)/Ni(III)	
	E_{pa}/V	E_{pc}/V	ΔE_p/V	$^{*}E_m$/V
GC	0.542	0.433	0.109	0.488
Pt	0.534	0.397	0.137	0.466
Au	0.630	0.456	0.174	0.543
ITO	0.593	0.439	0.154	0.516

* $E_m = (E_{pa} + E_{pc})/2$

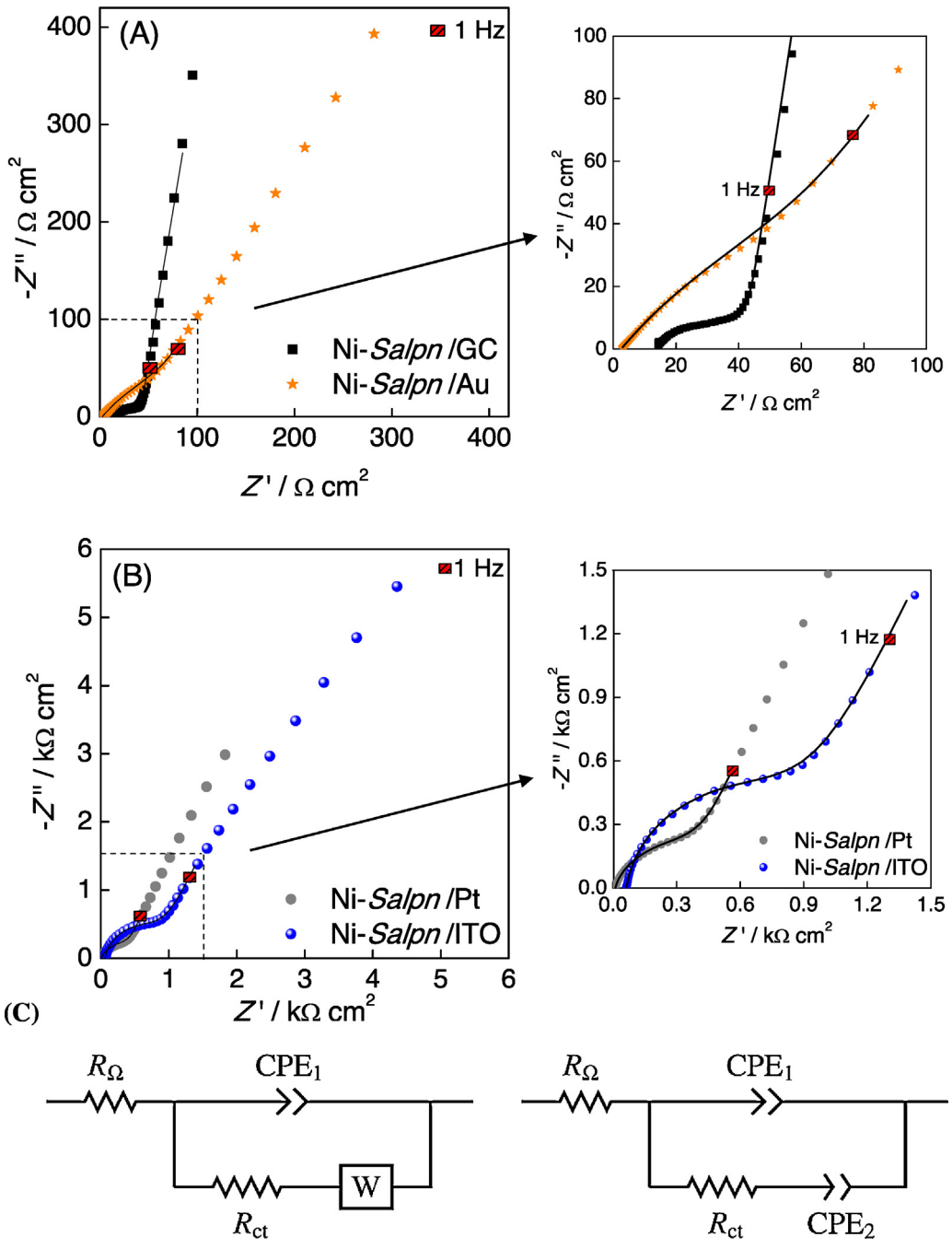

Fig. 3. Complex plane impedance spectra of (A) GC, Au, (B) Pt, and ITO electrodes modified with Ni-*Salpn* film, obtained in 0.1 mol L^{-1} KCl solution at OCP (+0.36 V *vs.* Ag/AgCl). Magnifications of the high frequency part are also shown. Lines indicate equivalent circuit fitting. (C) Equivalent electrical circuits.

transfer between the film and electrode surface. In fact, the current decreases less during the potential cycling of the modified GC and ITO electrodes, which can be explained by the nature of the interactions between the Ni-*Salpn* film and the electrode material, as follows. On the GC electrode surface chemical functionalities are present, such as quinones, ketones, alcohols, lactones and carboxylic acids as well as an aromatic network that provides electron delocalization [35,36]. Thus, radical attack can occur on the aromatic network of the GC electrode surface, changing the organization of π-bonds, thence influencing the interaction between the GC surface and the first layer of Ni-*Salpn*. Due to this interaction, Ni-*Salpn* films on the GC electrode cause a major effect on the rates of film growth and electron transfer as well as on the stability compared with the other electrode substrates used in this work. The ITO electrode showed similar behaviour to the metallic materials, which indicates that the oxide present on the glass surface does not provide strong interactions to maintain the stability of the film during the potential cycling in aqueous solution, as shown in Fig. 2c.

The cyclic voltammetry results show that the electrode material plays an important role on the stability of the Ni-*Salpn* film in aqueous solution.

3.2. Electrochemical impedance characterization of Ni-Salpn films

3.2.1. Influence of electrode material

EIS was used in order to evaluate the influence of the electrode material on the electrical properties of Ni-*Salpn* films. Impedance spectra, Fig. 3, were recorded in 0.1 mol L^{-1} KCl aqueous solution

Table 3
Parameters obtained from impedance spectra of the electrodes modified with Ni-*Salpn* film by fitting to the equivalent circuits of Fig. 4; frequency range 65 kHz to 1.0 Hz.

Substrate	R_Ω/Ω cm^2	CPE$_1$/μF cm^{-2} s$^{\alpha-1}$	α_1	R_{ct}/Ω cm^2	CPE$_2$/μF cm^{-2} s$^{\alpha-1}$	α_2	R_{diff} (W_o)/Ω cm^2	α_{Wo}
GC*	13.6	447	0.66	20.6	–	–	36.3	0.46
GC	13.6	504	0.64	21.2	–	–	30.6	0.44
Pt	11.5	42.6	0.85	278	–	–	601	0.38
Au	2.48	2141	0.55	215	1302	0.82	–	–
ITO	63.9	128	0.90	973	170	0.72	–	–

* Frequency range 65 kHz to 0.1 Hz

at open circuit potential (+0.36 V *vs.* Ag/AgCl (sat. KCl)), after electrodeposition of Ni-*Salpn* at a fixed potential of +1.2 V *vs.* Ag/AgCl during 900 s.

As seen in Fig. 3, all impedance spectra show a semicircle in the high frequency range that corresponds to kinetic control of the charge-transfer process, and a linear range at lower frequency, ascribed to diffusion control. However, the GC electrode modified with just the Ni-*Salpn* film showed good linearity for frequencies below 1 Hz. This behaviour suggests that the electrode material has a large influence on the electrical properties of the Ni-*Salpn* film.

The spectra were fitted to appropriate equivalent electrical circuits. The complex plane impedance spectra at GC and Pt electrodes modified with Ni-*Salpn* films were modelled using a typical Randles equivalent circuit consisting of the cell resistance, R_Ω, in series with a parallel combination of a constant phase element, CPE and a charge transfer resistance, R_{ct}, together with a Warburg impedance, Z_{wo} (finite diffusion) [37]. The CPE was modelled as a non-ideal capacitor, given by CPE = -1/(Ciω)$^\alpha$, where C is the capacitance, which describes the charge separation at the double layer interface, ω is the frequency in rad s^{-1} and α exponent is due to the heterogeneity of the surface ($0.5 < \alpha < 1$). The Warburg impedance was modelled as an open circuit finite Warburg element, resulting from the equation $Z_w = R_{dif}ctnh[(\tau i\omega)^\alpha]/(\tau i\omega)^\alpha$, where R_{dif} is the diffusion resistance of electroactive species, τ a time constant ($\tau = l^2/D$, where l is the effective diffusion thickness, and D is the effective diffusion coefficient of the species), and $\alpha < 0.5$. However, for modified Pt electrodes, this equivalent circuit could be applied only to higher frequencies (above 1 Hz). For the Au and ITO electrodes modified with Ni-*Salpn* film, changes to the equivalent circuit were necessary, where the Warburg impedance element was substituted with a CPE element, as shown in Fig. 3c. This change can occur when the counteranions impede diffusion, charge separation occurs and the interface acts as a non-ideal capacitor (CPE) [38,39]. Values of the circuit parameters are summarized in Table 3.

There is no direct relation between the values of the circuit parameters of the modified electrodes and film thickness, indicating that the behaviour of the Ni-*Salpn* films is associated principally with the intrinsic properties of the substrate electrode material. However, for the same electrode material, the thickness has a significant influence on the electrical properties and stability of the films, as described in subsections 3.2.2 and 3.4, respectively.

Comparing the values obtained for the charge transfer resistance, R_{ct}, the GC electrode modified with Ni-*Salpn* showed better conducting properties, which is in agreement with the results from cyclic voltammetry, suggesting that the glassy carbon surface allow a better interaction with the Ni-*Salpn* film. Furthermore, the modified GC electrode showed the small α exponent, that can be related to a greater heterogeneity of the film on the electrode surface. This facilitates counteranion diffusion into the stacked Ni-*Salpn* film structure, promoting a faster charge transfer process.

3.2.2. *Effect of electrodeposition parameters on GC electrodes*

Due to the greater reversibility and stability of the Ni-*Salpn* films on GC electrodes, the effect of electrodeposition parameters on the electrical properties in aqueous solution, were assessed by EIS at OCP, the Ni-*Salpn* films having been formed at a constant fixed potential of +1.0 V, +1.1 V or +1.2 V vs. Ag/AgCl for 900 s. As seen in Fig. 4a, all impedance spectra show a semicircle in the high frequency range that corresponds to kinetic control of the charge-transfer process, and a linear range at lower frequency, corresponding to diffusion control. The diameter of the semicircle, the charge transfer resistance, increases with an increase in the applied constant potential, which can be attributed to the increase in the amount of film electrodeposited on the electrode surface [27,40]. This can be related to the increase of the film thickness as well as to an increase of nucleation during the electrodeposition process.

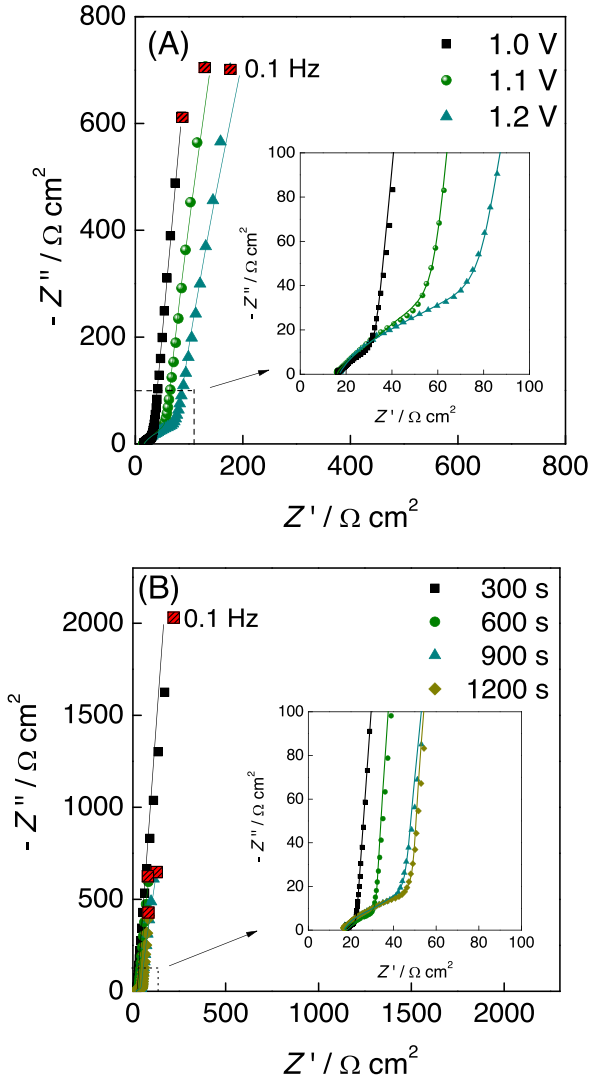

Fig. 4. Complex plane impedance spectra of GC electrodes modified with Ni-*Salpn* films in 0.1 mol L^{-1} KCl solution at OCP (+0.36 V *vs.* Ag/AgCl). Magnifications of the high frequency part are also shown. Lines indicate equivalent circuit fitting.
(A) For different electrodeposition potentials (+1.0 V, +1.1 V, +1.2 V *vs.* Ag/AgCl for 900 s), (B) For different electrodeposition times (300 s, 600 s and 900 s at +1.2 V *vs.* Ag/AgCl).

Table 4
Parameters obtained from impedance spectra at the GC electrode modified with Ni-*Salpn* film at different electrodeposition potentials, E_{dep}, and electrodeposition times, t_{dep}, by fitting to the equivalent circuits of Fig. 4.

Electrodeposition		$R_\Omega/\Omega\ cm^2$	$CPE_1/\mu F\ cm^{-2}\ s^{\alpha-1}$	α	$R_{ct}/\Omega\ cm^2$	$R_{dif}\ (W_o)/\Omega\ cm^2$	α_{Wo}
During 900 s	E_{dep}/V						
	+1.0	15.8	–	–	–	48.5	0.47
	+1.1	16.0	516	0.75	16.2	123	0.49
	+1.2	16.9	535	0.69	48.0	111	0.47
At + 1.2 V	t_{dep}/s						
	300	17.4	–	–	–	14.8	0.48
	600	17.1	450	0.75	7.80	28.6	0.49
	900	16.7	536	0.71	17.4	56.1	0.49
	1200	16.4	872	0.67	24.02	55.1	0.50

The parameters from equivalent circuit fitting are summarized in Table 4.

An increase in R_{ct} was also observed with increasing electrodeposition time at +1.2 V *vs.* Ag/AgCl, as shown in Fig. 4b and Table 4. However, for 1200 s electrodeposition time, hardly any variation in the diffusion impedance was seen in relation to 900 s, in agreement with cyclic voltammetry results. The same equivalent circuit was able to be applied to all the spectra, which suggests that the molecular organization of the Ni-*Salpn* film on the GC electrode surface is the same throughout the electrodeposition. As expected, the apparent charge transfer resistance and constant phase element depended on the amount of Ni-*Salpn* film electrodeposited on the electrode surface.

A decrease in the value of the CPE exponent α was observed with increasing electrodeposition potential and electrodeposition time, which indicates an increase in film roughness [25]. This is expected since the films from *Schiff* base complex form stack structures, so that a non-uniform film is obtained on the electrode surfaces. Therefore, the best electrical properties were observed with the Ni-*Salpn* films obtained by electrodeposition applying a potential of +1.2 V *vs.* Ag/AgCl for 900 s. In all cases, the Ni-*Salpn* film is unstable in aqueous solution, confirmed by a decrease in current with potential cycling.

Due to the instability in aqueous solution, impedance spectra were recorded at OCP after each potential cycle and for different times of immersion in aqueous solution, Fig. 5. Before potential cycling, the spectra of Ni-*Salpn* films showed behaviour that could be modelled by a Randles circuit, but after the fifth cycle in aqueous solution a significant change in both the low and high frequency range was observed, as shown in Fig. 5a.

The increase in semicircle diameter with potential cycling, as well as the decrease of peak current, observed by cyclic voltammetry (Fig. 2), suggests that ion diffusion from bulk electrolyte through the film as well as other effects, such as mass loss, blocks the redox process, since the profiles obtained until the last potential cycle are similar to those of unmodified GC.

To elucidate the effect of the insertion of the ion from bulk electrolyte into the Ni-*Salpn* film structure, the GC modified electrode was kept in 0.1 mol L^{-1} KCl solution and impedance spectra at OCP were recorded for different immersion times (Fig. 6b) together with cyclic voltammograms.

The increase in charge transfer resistance, R_{ct}, and the decrease in the value of CPE_1 with increasing immersion time, as shown in Fig. 6, can be ascribed to the loss of film due to ion insertion breaking bonds between the complexes in the stacked film structure, as shown in Scheme 1, and to the blockage of the redox metal centre by coordination with the counterion and/or solvent swelling inside the Ni-*Salpn* structure, as also observed by cyclic voltammetry. This suggests that mobile species insertion from bulk electrolyte to inside the film is constant with the time, but is not the only factor to block the redox process, where the mass loss also has a big influence, confirmed by EQCM measurements (see below).

The same behaviour was also observed for Ni-*Salpn* films formed on the other electrode materials. Thus, this effect can be due to intrinsic characteristics of the Ni-*Salpn* film and/or their interaction with the ions present in the supporting electrolyte.

3.3. Film growth assessed by UV-vis absorption spectroscopy

Shagisultanova and Ardasheva [41] affirmed that films obtained from Ni-*Salen* (*Salen*: *N*,*N*'-bis(salicylidene)ethylenediamine) and Ni-*Salphen* (*Salphen*:*N*,*N*'-bis(salicylidene)-*o*-phenylenediamine) complexes can grow on ITO by both continuous and stepwise

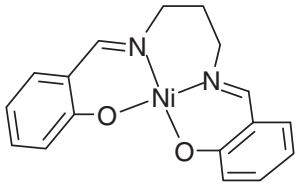

Ni-*Salpn*

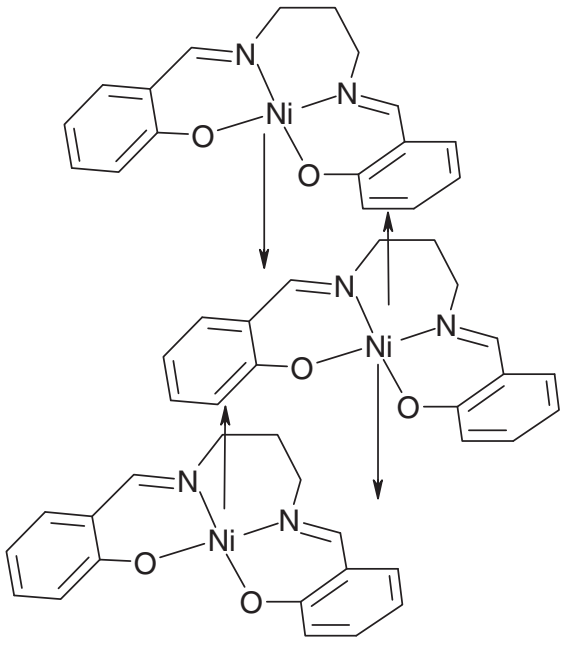

Ni-*Salpn* film

Scheme 1. Schematic representation of Ni-*Salpn* complexes (non-planar) and Ni-*Salpn* film.

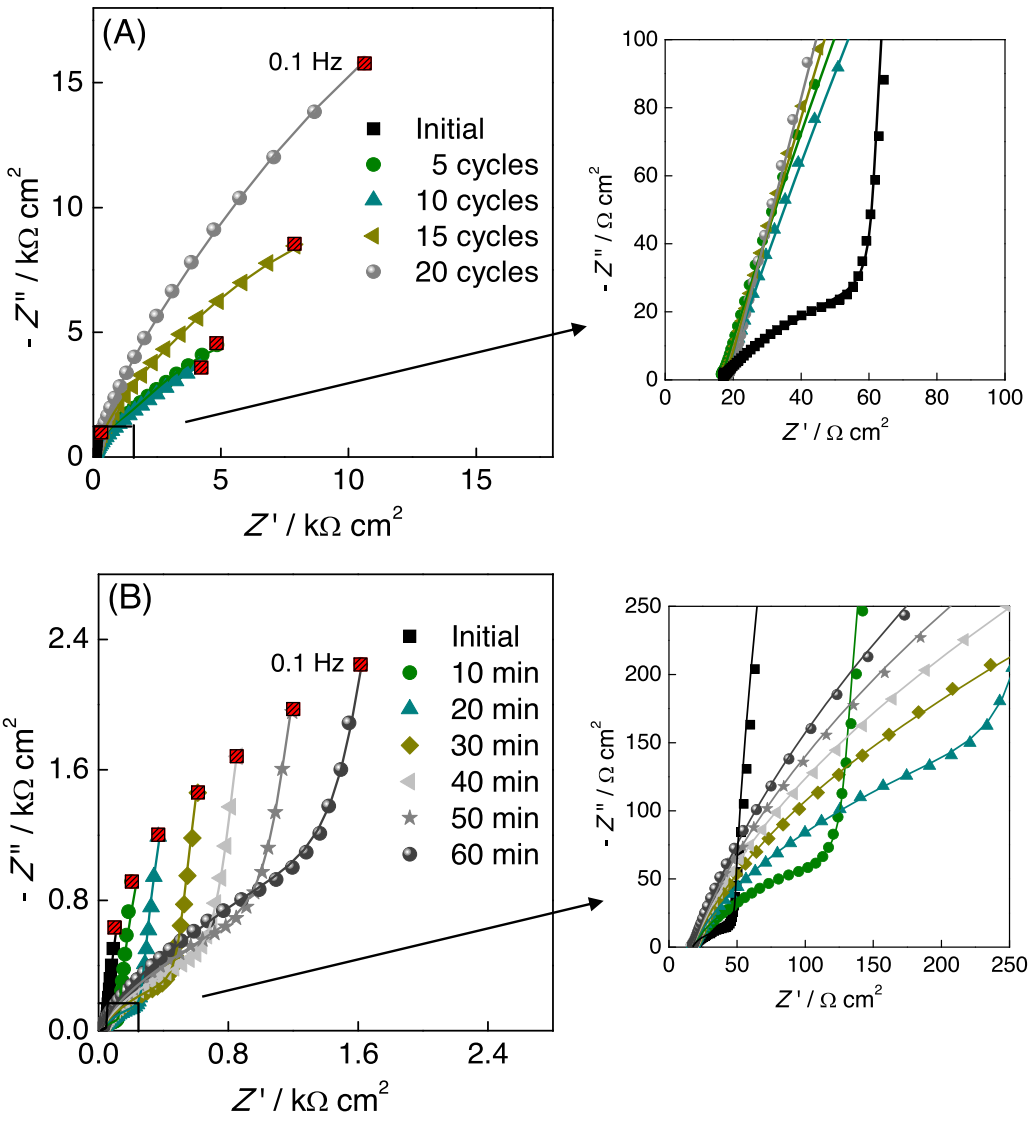

Fig. 5. Complex plane impedance spectra of GC electrodes modified with Ni-*Salpn* films in 0.1 mol L^{-1} KCl solution at OCP (+0.36 V *vs.* Ag/AgCl). Magnifications of the high frequency part are also shown. Lines indicate equivalent circuit fitting. (A) After potential cycling in 0.1 mol L^{-1} KCl solution at 25 mV s^{-1}. (B) After different immersion times in 0.1 mol L^{-1} KCl solution.

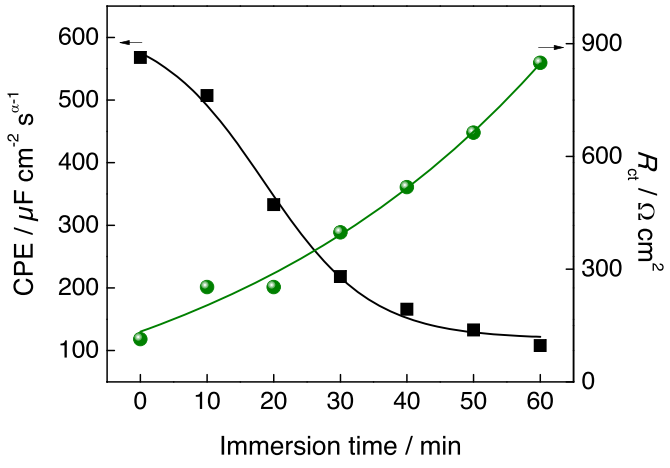

Fig. 6. Variation of CPE and R_{ct} values with immersion time in 0.1 mol L^{-1} KCl solution. Data from analysis of Fig. 5b.

electrodeposition, and that the film thickness is one of the most important parameters in the electron transfer process. Thus, the growth of Ni-*Salpn* on ITO electrode surfaces by electrodeposition at fixed constant potential for different times was monitored by UV-vis absorption spectroscopy, see Fig. 7. A linear increase of the absorbance at 377 nm with increase of electrodeposition time was observed, which indicates that the rate of electrodeposition was constant over the time range investigated.

The UV-vis absorption spectra of the Ni-*Salpn* film and of the Ni-*Salpn* complex in solution showed significant differences, which are attributed to particle aggregation with formation of conducting structures in the film [42]. Thus the absorbance band observed at 377 nm for the Ni-*Salpn* film can be attributed to the overlapping of the 352 and 421 nm absorption bands that the Ni-*Salpn* complex showed in dichloromethane (DCM) solution. This suggests that the molecular organization of the film occurs through the overlapping of the molecular orbitals, and all absorption bands observed in this spectral range are ascribed to charge transfer of the d_M-π_L^* type [42,43].

As described by Borisov *et al.* [42], the main spectral distinction between the oxidized and reduced forms of the Cu-*Salpn* film is that

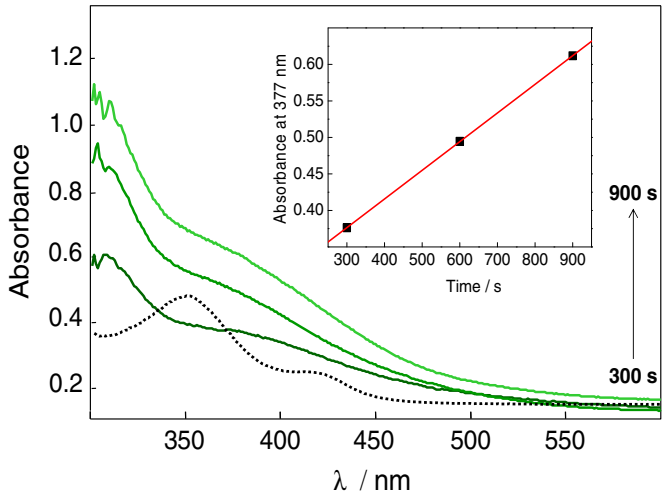

Fig. 7. UV-vis absorption spectra for Ni-*Salpn* films electrodeposited for different times on the ITO electrode. The dotted line corresponds to UV-vis absorption spectra of Ni-*Salpn*/DCM solution. In the inset are the values of absorbance at 377 nm *vs.* electrodeposition time.

broad absorption bands at wavelengths in the range 600–900 nm appear in the oxidized form and are eliminated in the reduced form. In this work, the UV-vis spectra were obtained for the Ni-*Salpn* film in its reduced form (stable form in oxidizing atmosphere), so that the band in the spectral range of 600-900 nm is not observed. However, the Ni-*Salpn* obtained for 900 s of electrodeposition showed a very low intensity broad absorption band centred at around 700 nm (data not shown), ascribed to d-d transitions [42]. This may occur due to the greater film thickness, where equilibrium of the oxidized and reduced species may exist between the inside of the Ni-*Salpn* film and its surface.

3.4. Gravimetric monitoring

The EQCM is an excellent technique to monitor film growth and evaluate the behaviour of the films whilst carrying out cyclic voltammetry. The variation of the frequency with time can be used to determine the change in mass during successive potential cycles, by using the Sauerbrey equation [44], for rigid films:

$$\Delta f = -\frac{2f_0^2}{A\sqrt{\mu_q \rho_q}}\Delta m$$

where f_0 is the resonant frequency (Hz), Δf is the frequency change (Hz), Δm is the mass change (g), A is the piezoelectrically active crystal area, ρ_q is the density of quartz (g cm^{-3}) and μ_q is the shear modulus of quartz for AT-cut crystals (g cm^{-1} s^{-2}). In the experimental arrangement in this study, the frequency/mass correlation factor is 1.102 kHz per 1 μg. The rigidity of the film was confirmed by the unchanging value of the dissipation factor during the gravimetric measurements (data not shown).

In the electrodeposition process at +1.2 V *vs.* Ag/AgCl during 900s on the AuQC, an immediate decrease of the frequency was observed, indicating fast nucleation of the Ni-*Salpn* complex on the AuQC surface, leading to rapid film growth [2,45]. The total frequency decrease after 900 s electrodeposition was Δf = 18.96 kHz, corresponding to a deposited mass of 17.2 μg. Cycling the potential of the Ni-*salpn*-coated AuQC in 0.1 mol L^{-1} KCl aqueous solution showed a decrease of mass, the decrease becoming almost zero after the 10th cycle, as shown in Fig. 8a. The mass loss after 15 cycles was 6.6 μg, leaving approximately 10.6 μg of Ni-*Salpn* film on the AuQC surface.

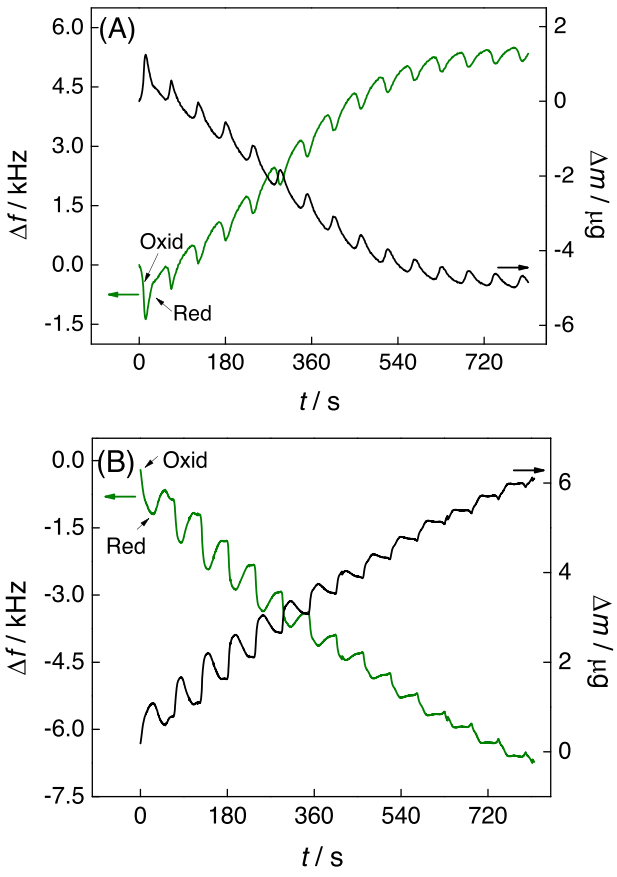

Fig. 8. Frequency and mass changes of Ni-*Salpn* film coated AuQC recorded in 0.1 mol L^{-1} KCl solution during potential cycling between +0.1 and +0.8 V *vs.* Ag/AgCl, for films electrodeposited during (A) 900 s and (B) 300 s.

For comparison, potential cycling of Ni-*salpn*-coated AuQC in 0.1 mol L^{-1} KCl aqueous solution, formed by electrodeposition during 300 s, corresponding to thinner Ni-*salpn* films was also done. The total deposited mass was 8.78 μg, that corresponds to ~50% of the mass deposited at 900s, indicating that film growth is not constant and is greater during the initial part of the electrodeposition process. For these thinner films, an increase of mass, rather than a decrease, was observed during potential cycling in aqueous solution, to be discussed further below.

Mass variation during the redox switching and cycling was observed for both films (formed during 300 s and 900 s). These aspects can be understood better by referring to Fig. 9.

A decrease of frequency during the positive sweep (above +0.5 V vs. Ag/AgCl), can be attributed to insertion of anions into the film structure, and an increase during the negative sweep (below +0.75 V vs. Ag/AgCl) to anion extraction, where the incorporation of anions is dominant, a mechanism essential for maintaining electroactivity [45,46].

In the first scan, for the Ni-*Salpn* film formed during 900s electrodeposition, the decrease of mass can be attributed to bond breaking as well as counterion insertion, which causes the greatest loss of film mass (see graphical abstract). This decrease in mass, due to bond breaking and loss of complex becomes less on further potential cycling, indicating a greater stability of the remaining film, as shown in Fig. 9A1 and A2. After 10 potential cycles, there is almost no change in frequency between successive cycles (up to 15 cycles); the intra-cycle variation can be attributed exclusively to anion insertion/expulsion. The crossover of the frequency *vs.* potential traces in the course of potential scan also indicates

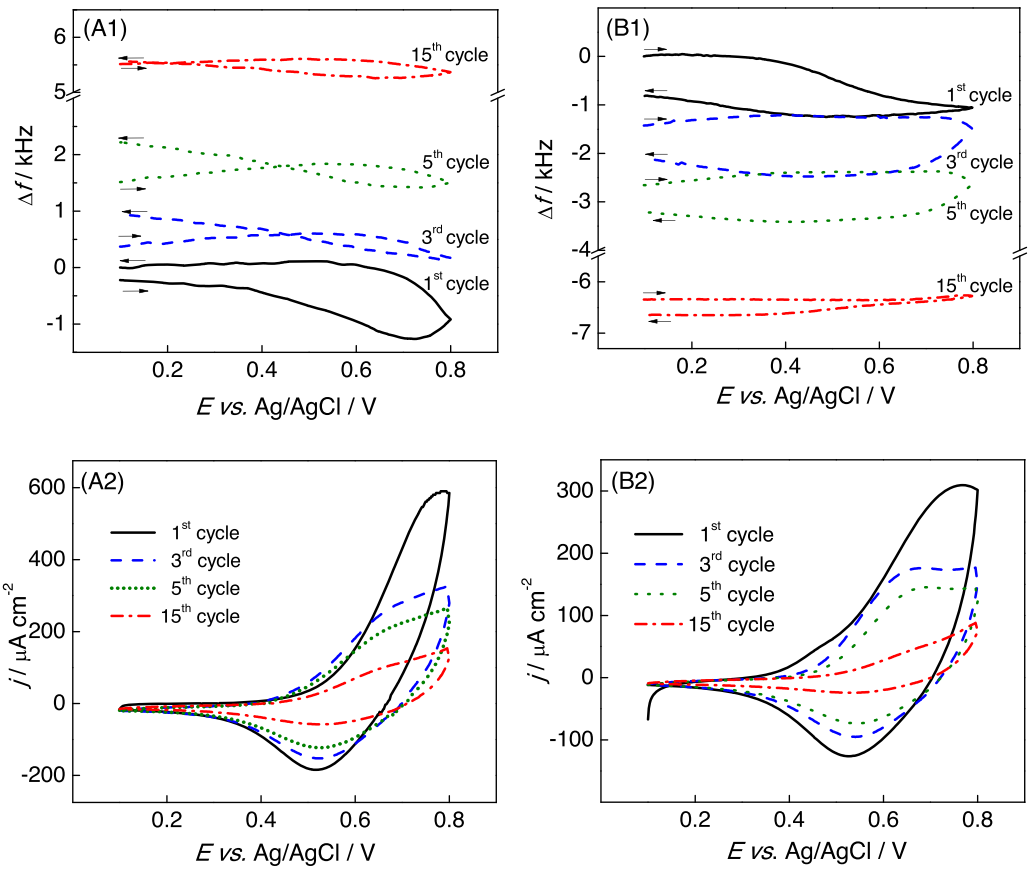

Fig. 9. Frequency changes and current response of Ni-*Salpn* film coated AuQC recorded in 0.1 mol L^{-1} KCl solution in the 1st, 3rd, 5th and 15th potential cycles during potential cycling between +0.1 and +0.8 V *vs.* Ag/AgCl for films electrodeposited during (A1) 900 s and (B1) 300 s, and their respective voltammograms (A2) and (B2).

that counteranion expulsion is more than its insertion, and which becomes smaller in successive potential scans.

Interestingly, gravimetric studies performed with the thinner Ni-*Salpn* films formed during 300s (Figs. 9 B1 and B2) showed an increase of mass which can be ascribed to net uptake of solvent within the Ni-*Salpn* film structure and very similar anion insertion/expulsion, with no crossover. This indicates a more stable structure of the thinner films; incorporation of solvent leads to swelling, as seen visually, and which is reversible.

The effect of structure on the electrodeposition mechanism, electrochemical behaviour and stability, has been widely discussed in the literature [16,17,47], and shows that the best properties are observed for films formed from symmetrical and planar *Schiff* base complexes, such as Ni(salen), where the films are formed through strong stacked acceptor-donor interactions. Vilas-Boas *et. al* [2,45] found that anion insertion into films formed by non-planar Ni(salen) derivatives causes structural changes, such as twisting. Consequently, the monomer units tend to align in a coplanar arrangement to maximize orbital overlap and promote charge delocalization through the film structure. Vilas-Boas *et. al* [1] also suggest that methyl (Me) groups present on the imine bridge of the 2,3-dimethyl-*N,N'-bis*(salicylidene)butane-2,3- diaminatonickel(II) (Ni-*SaltMe*) structure can provide repulsive forces, and would impose an open and flexible structure, responsible for facile anion ingress and solvent swelling. In comparison, Ni(*Salen*) shows a more compact structure, and the movement of species from solution into the film are associated solely with film charge transfer [1].

The Ni-*Salpn* complex has a non-planar structure [30], and the Ni-*Salpn* film is formed by weak orbital overlap, which can be broken by ion insertion and consequently loss of some layers from the film can occur. The propane ($-(CH_2)_3-$) bridge between the imine moieties can provide repulsive forces and impose an open film structure (Scheme 1), that facilitates anion insertion and solvent swelling. Therefore, a stable Ni-*Salpn* film can only be obtained when the film is very thin, in which the orbital overlap is more effective, the repulsion forces are minimized and the layers more compact. Thus, the mass loss from the Ni-*Salpn* film can be attributed to loss of Ni complexes during molecular rearrangement, as shown in Scheme 1.

According to the results obtained, the decrease of redox currents during oxidation and reduction of the Ni-*Salpn* films can be ascribed not only to mass change, but also to uptake of the counteranion and solvent within the Ni-*Salpn* film structure.

3.5. The counteranion effect

The separation of the counteranion and solvent contribution to electrochemical stability cannot be determined easily from the EQCM response alone, because the mass variation simultaneously reflects ion and solvent exchange. Thus, 15 potential cycles in various supporting electrolytes of concentration 0.1 mol L^{-1} with different anions Cl^-, NO_3^-, ClO_4^-, SO_4^{2-}, but the same cation (Na^+) were done in order to evaluate counteranion insertion within the Ni-*Salpn* film structure. It was found that the values of E_m are proportional to the ratio [ionic charge]/[ionic radius] of the anion present in solution for NO_3^-, ClO_4^- and SO_4^{2-}, Fig. 10, confirming the dependence on the mobility of the counterions of the supporting electrolyte in charge transport and in maintaining electroneutrality during potential cycling [1,2,46]. The higher value of E_m obtained for Cl^- ions compared with NO_3^-, which has a similar

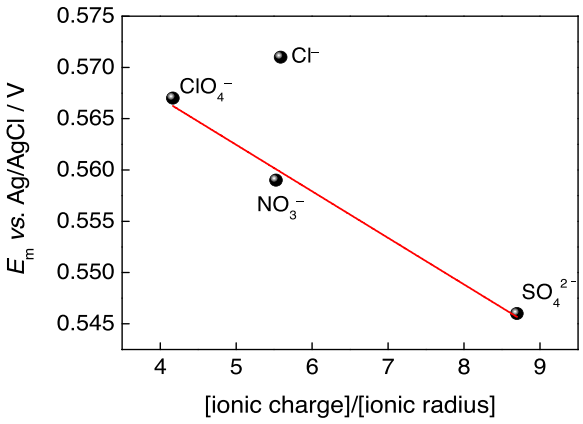

Fig. 10. Dependence of the mid-potential, E_m, of the GC electrode modified with Ni-*Salpn* thin film *vs.* [ionic charge]/[ionic radius] of counteranions. The values of ionic radius in aqueous solutions were from [48].

size [48], may indicate that Cl^- has a different interaction within the Ni-*Salpn* film structure.

3.6. Raman scattering

The Raman scattering technique was employed to follow the addition of the nickel metal ion to *Salpn* giving Ni-*Salpn* and its posterior electrodeposition as a Ni-*Salpn* film on ITO electrodes. The results obtained using a 633 nm excitation line are shown in Fig. 11. Significant changes between the *Salpn* ligand and Ni-*Salpn* complex spectra (both in powder form) were observed, such as shifting of bands to lower frequencies, such as the C=N stretching from 1632 to 1629 cm^{-1}, C=C stretching from 1583 to 1543 cm^{-1} and C–O_{phenyl} stretching from 1464 to 1454 cm^{-1}, as well as the appearance of new bands at 591 cm^{-1} and 458 cm^{-1} ascribed to Ni–N and Ni–O stretching, respectively [49–52]. The latter is consistent with the insertion of nickel in the N_2O_2 coordination centre of the *Salpn* ligand [53]. The C=C and C=N bands, at ca. 1543 and 1629 cm^{-1}, decrease in intensity after electrodeposition owing to a decrease in π delocalisation, and a new band at ca. 1603 cm^{-1} appears, attributed to C-C bonds in the propane (–$(CH_2)_3$–) bridge between the imine moieties (Fig. 11) [54].

All the differences between the spectra of Ni-*Salpn* powder and Ni-*Salpn* film can be attributed to the electropolymerisation through stacked acceptor-donor interactions [10,12], such as

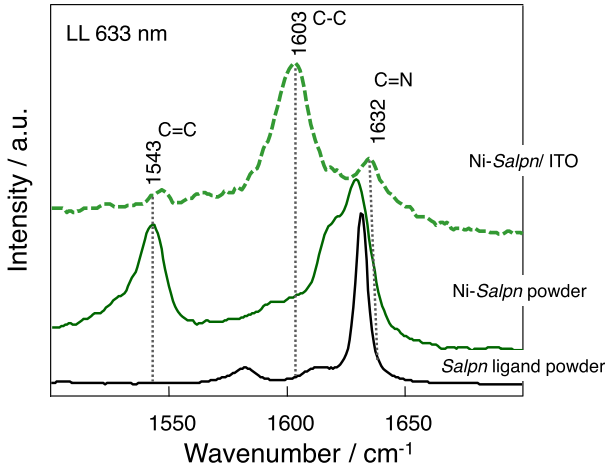

Fig. 11. Raman spectrum for Ni-*Salpn* film on ITO electrode surface, Ni-*Salpn* complex (powder) and *Salpn* ligand (powder), recorded using the 633 nm laser line. Spectrum range from 1500 cm^{-1} to 1700 cm^{-1}.

broadening and decreasing of the bands due to the less localized vibrations in the polymer than in the monomer [55].

4. Conclusions

The mechanism of Ni-*Salpn* film formation by electrodeposition in 1,2-dichloroethane occurs via the overlapping of the orbitals of the aromatic rings of one monomer molecule with the metallic centre of other monomers present in solution, which is independent of the electrode material. However, the electrode material showed a big influence on the rate of film growth as well as on the electrochemical behaviour and stability of the films in aqueous solution. Due to the non-planar structure of the Ni-*Salpn* complexes, the Ni-*Salpn* films are formed through weak interactions, and counteranion insertion during oxidation leads to breaking of the bonds between the complexes in the stacked Ni-*Salpn* film structure, which causes mass loss. Moreover, the propane (–$(CH_2)_3$–) bridge between the imine moieties can lead to repulsive forces and impose an open structure on the film, that facilitates anion and solvent uptake, and consequent blockage of the redox metal centre. The thinner Ni-*Salpn* films have a more effective orbital overlap and a more compact stacked structure, being more stable in aqueous solution and showing the most promising electrochemical properties as modified electrodes for sensing applications.

Acknowledgements

Financial support from Fundação para a Ciência e a Tecnologia (FCT), Portugal PTDC/QUI-QUI/116091/2009, POPH, POCH, POFC-QREN (co-financed by FSE and European Community FEDER funds through the program COMPETE - Programa Operacional Factores de Competitividade under the projects PEst-C/EME/UI0285/2013 and CENTRO-07-0224-FEDER-002001 (MT4MOBI)) is gratefully acknowledged. C.S.M. thanks FAPESP for doctoral fellowships 2012/25140-7 and 2013/22087-0. C.G.C. thanks FCT for post-doctoral fellowship SFRH/BPD/46635/2008.

References

[1] M. Vilas-Boas, C. Freire, B. de Castro, P.A. Christensen, A.R. Hillman, Spectroelectrochemical characterisation of poly[Ni(saltMe)]-modified electrodes, Chem. Eur. J. 7 (2001) 139.
[2] M. Vilas-Boas, I.C. Santos, M.J. Henderson, C. Freire, A.R. Hillman, E. Vieil, Electrochemical behavior of a new precursor for the design of poly[Ni(*salen*)]-based modified electrodes, Langmuir 19 (2003) 7460.
[3] O. Fatibello, E.R. Dockal, L.H. Marcolino, Electrochemical modified electrodes based on metal-*Salen* complexes, Anal. Lett. 40 (2007) 1825.
[4] C.S. Martin, T.R.L. Dadamos, M.F.S. Teixeira, Development of an electrochemical sensor for determination of dissolved oxygen by nickel–*salen* polymeric film modified electrode, Sensor. Actuat. B-Chem. 175 (2012) 111.
[5] K.A. Goldsby, J.K. Blaho, L.A. Hoferkamp, Oxidation of nickel(II) bis(salicylaldimine) complexes: solvent control of the ultimate redox site, Polyhedron 8 (1989) 113.
[6] K.A. Goldsby, Symmetric and unsymmetric nickel(II) *Schiff* base complexes; metal-localized versus ligand-localized oxidation, J. Coord. Chem. 19 (1988) 83.
[7] P. Audebert, P. Capdevielle, M. Maumy, Synthesis and characteristics of new redox polymers based on copper containing units; evidence for the participation of copper in the electron transfer mechanism, New J. Chem. 15 (1991) 235.
[8] P. Audebert, P. Capdevielle, M. Maumy, Description of new redox and conducting polymers based on copper containing units; emphasis on the role of copper in the electron transfer mechanism, Synthetic Met. 43 (1991) 3049.
[9] P. Audebert, P. Capdevielle, M. Maumy, Redox and conducting polymers based on *Salen*-type metal units; electrochemical study and some characteristics, New J. Chem. 16 (1992) 697.
[10] M. Vilas-Boas, C. Freire, B. de Castro, P.A. Christensen, A.R. Hillman, New insights into the structure and properties of electroactive polymer films derived from [Ni(*salen*)], Inorg. Chem. 36 (1997) 4919.
[11] M. Vilas-Boas, C. Freire, B. de Castro, A.R. Hillman, Electrochemical characterization of a novel *Salen*-type modified electrode, J. Phys. Chem. B 102 (1998) 8533.
[12] C.E. Dahm, D.G. Peters, J. Simonet, Electrochemical and spectroscopic characterization of anodically formed nickel *salen* polymer films on glassy carbon,

platinum, and optically transparent tin oxide electrodes in acetonitrile containing tetramethylammonium tetrafluoroborate, J. Electroanal. Chem. 410 (1996) 163.
[13] Z.J. Zhang, X. Li, C.G. Wang, C.C. Zhang, P. Liu, T.T. Fang, Y. Xiong, W.J. Xu, A novel dinuclear *Schiff*-base copper(II) complex modified electrode for ascorbic acid catalytic oxidation and determination, Dalton Trans. 41 (2012) 1252.
[14] T.R.L. Dadamos, M.F.S. Teixeira, Electrochemical sensor for sulfite determination based on a nanostructured copper-*salen* film modified electrode, Electrochim. Acta 54 (2009) 4552.
[15] M. Motaghedifard, M. Behpour, S.M. Ghoreishi, Self-assembling monolayer of *Schiff*'s base formed between o-methoxyphenyl methyl ketone and 2-aminothiophenol at the surface of gold electrode for electrochemical impedimetric sensing of uranyl cations, Sensor. Actuat. B-Chem. 203 (2014) 802.
[16] J.L. Reddinger, J.R. Reynolds, Tunable redox and optical properties using transition metal-complexed polythiophenes, Macromolecules 30 (1997) 673–675.
[17] J.L. Reddinger, J.R. Reynolds, Site specific electropolymerization to form transition-metal-containing, electroactive polythiophenes, Chem. Mat. 10 (1998) 1236.
[18] J.L. Li, F. Gao, Y.K. Zhang, L.Z. He, G.M. Han, X.D. Wang, Electropolymerization of nickel complexes with *Schiff* bases: effect of sweep rate on anodic polymerization, Acta Phys-Chim.Sin. 26 (2010) 2647.
[19] L.P. Ardasheva, G.V. Vovk, L.G. Pchelova, G.A. Shagisultanova, Anodic electrochemical polymerization of complexes [Ni(*Salpn*-1,3)] and [Cu(Salpn-1,3)], Russ. J. Appl. Chem. 77 (2004) 1962.
[20] R. Kurtaran, L.T. Yildirim, A.D. Azaz, H. Namli, O. Atakol, Synthesis, characterization, crystal structure and biological activity of a novel heterotetranuclear complex: $[NiLPb(SCN)_2(DMF)(H_2O)]_2$, bis-{[μ-*N,N'*-bis(salicylidene)-1,3-propanediaminato-aqua-nickel(II)](thiocyanato)(μ-thiocyanato)(μ-*N,N'*-dimethylformamide)lead(II)}, J. Inorg. Biochem. 99 (2005) 1937.
[21] E. Kormali, E. Kilic, N,N'-disalicylidene-1,3-diaminopropane as a selective chelating titrant for copper(II), Talanta 58 (2002) 793.
[22] K.J. Schenk, S. Meghdadi, M. Amirnasr, M.H. Habibi, A. Amiri, M. Salehi, A. Kashi, Co(III) complexes of Me-salpn and Me-salbn and the ring size effect on the coordination modes and electrochemical properties: The crystal structures of *trans*-$[Co^{III}(Me\text{-}salpn)(py)_2]PF_6$ and *cis*-α-$[Co^{III}(Me\text{-}salbn)(4\text{-}Mepy)_2]BPh_4 \cdot 4\text{-}Mepy$, Polyhedron. 26 (2007) 5448.
[23] M. Maneiro, M.R. Bermejo, A. Sousa, M. Fondo, A.M. González, A. Sousa-Pedrares, C.A. McAuliffe, Synthesis and structural characterisation of new manganese(II) and (III) complexes. Study of their photolytic and catalase activity and X-ray crystal structure of $[Mn(3\text{-}OMe, 5\text{-}Br\text{-}salpn)(EtOH)(H_2O)]ClO_4$, Polyhedron 19 (2000) 47.
[24] S.M. Chen, C.J. Liao, V.S. Vasantha, Preparation and electrocatalytic properties of osmium oxide/hexacyanoruthenate films modified electrodes for catecholamines and sulfur oxoanions, J. Electroanal. Chem. 589 (2006) 15.
[25] E. Telli, A. Doner, G. Kardas, Electrocatalytic oxidation of methanol on Ru deposited NiZn catalyst at graphite in alkaline medium, Electrochim. Acta 107 (2013) 216.
[26] A.A. Isse, A. Gennaro, E. Vianello, Mechanism of the electrochemical reduction of benzyl chlorides catalysed by Co(*salen*), J. Electroanal.Chem. 444 (1998) 241.
[27] D.M. Fernandes, M.E. Ghica, A.M.V. Cavaleiro, C.M.A. Brett, Electrochemical impedance study of self-assembled layer-by-layer iron–silicotungstate/poly(ethylenimine) modified electrodes, Electrochim. Acta 56 (2011) 7940.
[28] S.R. Gupta, P. Mourya, M.M. Singh, V.P. Singh, Synthesis, structural, electrochemical and corrosion inhibition properties of two new ferrocene *Schiff* bases derived from hydrazides, J. Organomet. Chem. 767 (2014) 136.
[29] E.M. Pinto, M.M. Barsan, C.M.A. Brett, Mechanism of formation and construction of self-assembled myoglobin/hyaluronic Acid Multilayer Films: An Electrochemical QCM, Impedance, and AFM Study, J. Phys. Chem. B 114 (2010) 15354.
[30] O. Atakol, H. Nazir, C. Arici, S. Durmus, I. Svoboda, H. Fuess, Some new Ni–Zn heterodinuclear complexes: square-pyramidal nickel(II) coordination, Inorg. Chim. Acta 342 (2003) 295.
[31] Y.K. Zhang, J.L. Li, F. Gao, F.Y. Kang, X.D. Wang, F. Ye, J. Yang, Electropolymerization and electrochemical performance of *salen*-type redox polymer on different carbon supports for supercapacitors, Electrochim. Acta 76 (2012) 1.
[32] A.M. Couper, D. Pletcher, F.C. Walsh, Electrode materials for electrosynthesis, Chem. Rev. 90 (1990) 837.
[33] U. Oesch, J. Janata, Electrochemical study of gold electrodes with anodic oxide films-ii. Inhibition of electrochemical redox reactions by monolayers of surface oxides, Electrochim. Acta 28 (1983) 1247.
[34] A.J. Bard, L.R. Faulkner, Electrochemical methods: fundamentals and applications, 2nd ed., Wiley, New York, 2001.
[35] C.A. Thorogood, G.G. Wildgoose, J.H. Jones, R.G. Compton, Identifying quinone-like species on the surface of graphitic carbon and multi-walled carbon nanotubes using reactions with 2,4-dinitrophenylhydrazine to provide a voltammetric fingerprint, New J. Chem. 31 (2007) 958.
[36] B. Uslu, S.A. Ozkan, Electroanalytical application of carbon based electrodes to the pharmaceuticals, Anal. Lett. 40 (2007) 817.
[37] C.M.A. Brett, A.M. Oliveira-Brett, Electrochemistry: principles, methods, and applications, Oxford University Press, Oxford, 1993.
[38] P.A. Ahn, E.C. Shin, G.R. Kim, J.S. Lee, Application of generalized transmission line models to mixed ionic-electronic transport phenomena, J. Korean Ceram. Soc. 48 (2011) 549.
[39] J. Bisquert, G. Garcia-Belmonte, P. Bueno, E. Longo, L.O.S. Bulhoes, Impedance of constant phase element (CPE) -blocked diffusion in film electrodes, J. Electroanal. Chem. 452 (1998) 229.
[40] C. Wang, A.J. Appleby, F.E. Little, Charge–discharge stability of graphite anodes for lithium-ion batteries, J. Electroanal. Chem. 497 (2001) 33.
[41] G.A. Shagisultanova, L.P. Ardasheva, Electrochemical synthesis of thin films of polymers derived from [Ni*Salen*] and [Ni*Salphen*], Russ. J. Appl. Chem. 76 (2003) 1626.
[42] A.N. Borisov, A.V. Shchukarev, G.A. Shagisultanova, A new conducting polymer based on the complex of Cu(II) with *N,N'*-bis(3-methoxysalicylidene)-1,3-propylenediamine, Russ. J. Appl. Chem. 82 (2009) 1242.
[43] I. Alan, A. Kriza, R. Olar, N. Stanica, M. Badea, Spectral, magnetic and thermal characterisation of new Co(II), Ni(II) and Cu(II) complexes with *Schiff* base 5-bromo-*N,N'*-bis-(salicylidene)-o-toluidine, J. Therm. Anal. Calorim. 111 (2013) 1163.
[44] G. Sauerbrey, Verwendung von Schwingquarzen zur Wägung dünner Schichten und zur Mikrowägung, Z. Phys 155 (1959) 206.
[45] M. Vilas-Boas, M.J. Henderson, C. Freire, A.R. Hillman, E. Vieil, A combined electrochemical quartz-crystal microbalance probe beam deflection (EQCM-PBD) study of solvent and ion transfer at a poly[Ni(saltMe)]-modified electrode during redox switching, Chem. Eur. J. 6 (2000) 1160.
[46] V.V. Sizov, M.V. Novozhilova, E.V. Alekseeva, M.P. Karushev, A.M. Timonov, S.N. Eliseeva, A.A. Vanin, V.V. Malev, O.V. Levin, Redox transformations in electroactive polymer films derived from complexes of nickel with SalEn-type ligands: computational, EQCM, and spectroelectrochemical study, J. Solid. State. Electrochem. 19 (2014) 453.
[47] L. Marin, V. Harabagiu, A. Van Der Lee, A. Arvinte, M. Barboiu, Structure-directed functional properties of symmetrical and unsymmetrical Br-substituted *Schiff*-bases, J. Mol. Struct. 1049 (2013) 377.
[48] Y. Marcus, Ionic radii in aqueous solution, Chem. Rev. 88 (1988) 1475.
[49] D. Lin-Vien, The handbook of infrared and Raman characteristic frequencies of organic molecules, Academic Press, Boston, 1991.
[50] I. Alan, A. Kriza, R. Olar, N. Stanica, M. Badea, Spectral, magnetic and thermal characterisation of new Co(II), Ni(II) and Cu(II) complexes with *Schiff* base 5-bromo-*N,N'-bis-(salicylidene)*-o-*tolidine*, J. Therm. Anal. Calorim. 111 (2013) 1163.
[51] R.C. Felicio, E.T.G. Cavalheiro, E.R. Dockal, Preparation, characterization and thermogravimetric studies of [*N,N'-cis*-1,2-cyclohexylene bis(salicylideneaminato)] cobalt(II) and [N,N'-(±)-trans-1,2-cyclo-hexylene bis(salicylideneaminato)]cobalt(II), Polyhedron 20 (2001) 261.
[52] M.R. Maurya, S.J.J. Titinchi, S. Chand, I.M. Mishra, Zeolite-encapsulated Cr(III), Fe(III), Ni(II), Zn(II) and Bi(III) *salpn* complexes as catalysts for the decomposition of H_2O_2 and oxidation of phenol, J. Molec. Catal. A: Chem. 180 (2002) 201.
[53] P.E. Aranha, M.P. Dos Santos, S. Romera, E.R. Dockal, Synthesis, characterization, and spectroscopic studies of tetradentate *Schiff* base chromium(III) complexes, Polyhedron 26 (2007) 1373.
[54] R. Das, K. Kumar, Vibrational spectra and Raman excitation profiles of some *Schiff* bases, Spectrochim. Acta A. 45 (1989) 705.
[55] D.L. Chinaglia, C.J.L. Constantino, R.F. Aroca, O.N. Oliveira Jr., Surface modifications on Teflon FEP and Mylar C induced by a low energy electron beam: a Raman and FTIR spectroscopy study, Mol. Cryst. Liq. Cryst 374 (2002) 577.